Measurement of the Proton Spin Structure Function $g_1(x,Q^2)$ for Q^2 from 0.15 to 1.6 GeV^2 with CLAS

R. Fatemi,[37] A.V. Skabelin,[21] V.D. Burkert,[35] D. Crabb,[37] R. De Vita,[16] S.E. Kuhn,[27] R. Minehart,[37] G. Adams,[29] E. Anciant,[6] M. Anghinolfi,[16] B. Asavapibhop,[22] G. Audit,[6] T. Auger,[6] H. Avakian,[15, 35] H. Bagdasaryan,[39] J.P. Ball,[2] S. Barrow,[12] M. Battaglieri,[16] K. Beard,[19] M. Bektasoglu,[27] M. Bellis,[29] W. Bertozzi,[21] N. Bianchi,[15] A.S. Biselli,[29] S. Boiarinov,[35] B.E. Bonner,[30] P.E. Bosted,[1] S. Bouchigny,[17] R. Bradford,[4] D. Branford,[10] W.K. Brooks,[35] C. Butuceanu,[38] J.R. Calarco,[24] D.S. Carman,[26] B. Carnahan,[5] C. Cetina,[13] L. Ciciani,[27] R. Clark,[4] P.L. Cole,[34] A. Coleman,[38] J. Connelly,[13] D. Cords,[35, *] P. Corvisiero,[16] H. Crannell,[5] J.P. Cummings,[29] E. De Sanctis,[15] P.V. Degtyarenko,[35] H. Denizli,[28] L. Dennis,[12] K.V. Dharmawardane,[27] K.S. Dhuga,[13] C. Djalali,[32] G.E. Dodge,[27] D. Doughty,[7] P. Dragovitsch,[12] M. Dugger,[2] S. Dytman,[28] M. Eckhause,[38] H. Egiyan,[38] K.S. Egiyan,[39] L. Elouadrhiri,[35] A. Empl,[29] P. Eugenio,[12] L. Farhi,[6] R.J. Feuerbach,[4] A. Freyberger,[35] J. Ficenec,[36] T.A. Forest,[27] V. Frolov,[29] H. Funsten,[38] S.J. Gaff,[9] M. Gai,[8] M. Garçon,[6] G. Gavalian,[24] S. Gilad,[21] G.P. Gilfoyle,[31] K.L. Giovanetti,[19] P. Girard,[32] C.I.O. Gordon,[14] K.A. Griffioen,[38] M. Guidal,[17] M. Guillo,[32] L. Guo,[35] V. Gyurjyan,[35] C. Hadjidakis,[17] D. Hancock,[38] J. Hardie,[7] D. Heddle,[7] P. Heimberg,[13] F.W. Hersman,[24] K. Hicks,[26] R.S. Hicks,[22] M. Holtrop,[24] J. Hu,[29] C.E. Hyde-Wright,[27] Y. Ilieva,[13] M.M. Ito,[35] D. Jenkins,[36] K. Joo,[35] C. Keith,[35] J.H. Kelley,[9] J.D. Kellie,[14] M. Khandaker,[25] K.Y. Kim,[28] K. Kim,[20] W. Kim,[20] A. Klein,[27] F.J. Klein,[5] A.V. Klimenko,[27] M. Klusman,[29] M. Kossov,[18] V. Koubarovski,[29] L.H. Kramer,[11] Y. Kuang,[38] J. Kuhn,[29] J. Lachniet,[4] J.M. Laget,[6] D. Lawrence,[22] Ji Li,[29] K. Livingston,[14] A. Longhi,[5] K. Lukashin,[35] W. Major,[31] J.J. Manak,[35] C. Marchand,[6] S. McAleer,[12] J.W.C. McNabb,[4] B.A. Mecking,[35] S. Mehrabyan,[28] M.D. Mestayer,[35] C.A. Meyer,[4] K. Mikhailov,[18] M. Mirazita,[15] R. Miskimen,[22] L. Morand,[6] S.A. Morrow,[17] V. Muccifora,[15] J. Mueller,[28] G.S. Mutchler,[30] J. Napolitano,[29] R. Nasseripour,[11] S.O. Nelson,[9] S. Niccolai,[13] G. Niculescu,[26] I. Niculescu,[13] B.B. Niczyporuk,[35] R.A. Niyazov,[27] M. Nozar,[35] J.T. O'Brien,[5] G.V. O'Rielly,[13] M. Osipenko,[16, 23] K. Park,[20] E. Pasyuk,[2] G. Peterson,[22] N. Pivnyuk,[18] D. Pocanic,[37] O. Pogorelko,[18] E. Polli,[15] S. Pozdniakov,[18] B.M. Preedom,[32] J.W. Price,[3] Y. Prok,[37] D. Protopopescu,[24] L.M. Qin,[27] B.A. Raue,[11] G. Riccardi,[12] G. Ricco,[16] M. Ripani,[16] B.G. Ritchie,[2] S.E. Rock,[1] F. Ronchetti,[15] P. Rossi,[15] D. Rowntree,[21] P.D. Rubin,[31] F. Sabatié,[6] K. Sabourov,[9] C. Salgado,[25] J.P. Santoro,[36] V. Sapunenko,[16] M. Sargsyan,[11] R.A. Schumacher,[4] M. Seely,[35] V.S. Serov,[18] Y.G. Sharabian,[35] J. Shaw,[22] S. Simionatto,[13] E.S. Smith,[35] T. Smith,[24] L.C. Smith,[37] D.I. Sober,[5] L. Sorrel,[1] M. Spraker,[9] A. Stavinsky,[18] S. Stepanyan,[27] P. Stoler,[29] S. Strauch,[13] M. Taiuti,[16] S. Taylor,[30] D.J. Tedeschi,[32] U. Thoma,[35] R. Thompson,[28] L. Todor,[4] C. Tur,[32] M. Ungaro,[29] M.F. Vineyard,[33] A.V. Vlassov,[18] K. Wang,[37] L.B. Weinstein,[27] H. Weller,[9] D.P. Weygand,[35] C.S. Whisnant,[19] E. Wolin,[35] M.H. Wood,[32] A. Yegneswaran,[35] J. Yun,[27] B. Zhang,[21] J. Zhao,[21] and Z. Zhou[21]

(The CLAS Collaboration)

[1] *American University, Washington, DC 20016*
[2] *Arizona State University, Tempe, Arizona 85287-1504*
[3] *University of California at Los Angeles, Los Angeles, California 90095-1547*
[4] *Carnegie Mellon University, Pittsburgh, Pennsylvania 15213*
[5] *Catholic University of America, Washington, D.C. 20064*
[6] *CEA-Saclay, Service de Physique Nucléaire, F91191 Gif-sur-Yvette, Cedex, France*
[7] *Christopher Newport University, Newport News, Virginia 23606*
[8] *University of Connecticut, Storrs, Connecticut 06269*
[9] *Duke University, Durham, North Carolina 27708-0305*
[10] *Edinburgh University, Edinburgh EH9 3JZ, United Kingdom*
[11] *Florida International University, Miami, Florida 33199*
[12] *Florida State University, Tallahassee, Florida 32306*
[13] *The George Washington University, Washington, DC 20052*
[14] *University of Glasgow, Glasgow G12 8QQ, United Kingdom*
[15] *INFN, Laboratori Nazionali di Frascati, Frascati, Italy*
[16] *INFN, Sezione di Genova, 16146 Genova, Italy*
[17] *Institut de Physique Nucleaire ORSAY, Orsay, France*
[18] *Institute of Theoretical and Experimental Physics, Moscow, 117259, Russia*
[19] *James Madison University, Harrisonburg, Virginia 22807*
[20] *Kyungpook National University, Daegu 702-701, South Korea*
[21] *Massachusetts Institute of Technology, Cambridge, Massachusetts 02139-4307*
[22] *University of Massachusetts, Amherst, Massachusetts 01003*
[23] *Moscow State University, Moscow, 119899, Russia*

^{24} *University of New Hampshire, Durham, New Hampshire 03824-3568*
^{25} *Norfolk State University, Norfolk, Virginia 23504*
^{26} *Ohio University, Athens, Ohio 45701*
^{27} *Old Dominion University, Norfolk, Virginia 23529*
^{28} *University of Pittsburgh, Pittsburgh, Pennsylvania 15260*
^{29} *Rensselaer Polytechnic Institute, Troy, New York 12180-3590*
^{30} *Rice University, Houston, Texas 77005-1892*
^{31} *University of Richmond, Richmond, Virginia 23173*
^{32} *University of South Carolina, Columbia, South Carolina 29208*
^{33} *Union College, Schenectady, New York 12308*
^{34} *University of Texas at El Paso, El Paso, Texas 79968*
^{35} *Thomas Jefferson National Accelerator Facility, Newport News, Virginia 23606*
^{36} *Virginia Polytechnic Institute and State University, Blacksburg, Virginia 24061-0435*
^{37} *University of Virginia, Charlottesville, Virginia 22901*
^{38} *College of Willliam and Mary, Williamsburg, Virginia 23187-8795*
^{39} *Yerevan Physics Institute, 375036 Yerevan, Armenia*
(Dated: February 4, 2008)

Double-polarization asymmetries for inclusive *ep* scattering were measured at Jefferson Lab using 2.6 and 4.3 GeV longitudinally polarized electrons incident on a longitudinally polarized NH$_3$ target in the CLAS detector. The polarized structure function $g_1(x, Q^2)$ was extracted throughout the nucleon resonance region and into the deep inelastic regime, for $Q^2 = 0.15 - 1.64$ GeV^2. The contributions to the first moment $\Gamma_1(Q^2) = \int g_1(x, Q^2)dx$ were determined up to $Q^2 = 1.2$ GeV^2. Using a parametrization for g_1 in the unmeasured low x regions, the complete first moment was estimated over this Q^2 region. A rapid change in Γ_1 is observed for $Q^2 < 1$ GeV^2, with a sign change near $Q^2 = 0.3$ GeV^2, indicating dominant contributions from the resonance region. At $Q^2 = 1.2$ GeV^2 our data are below the pQCD evolved scaling value.

PACS numbers: 13.40.Gp, 13.60.Hb, 14.20.Dh

Electron scattering has played a long and distinguished role in the study of nucleon structure. Inclusive deep inelastic scattering (DIS) studies [1] revealed the parton constituents (quarks and gluons) of the nucleon. At low values of the four momentum transfer Q^2 the nucleon structure functions depend on both Q^2 and on the energy transfer $\nu = E_0 - E'$, where E_0 and E' are the initial and final electron energies. In the asymptotic limit, $Q^2 \rightarrow \infty$, the scattering is described by perturbative Quantum Chromodynamics (pQCD) as the absorption of a virtual photon on a single free quark. In this limit the structure functions depend only on the Bjorken scaling variable, $x = Q^2/2M\nu$, where M is the nucleon mass.

When both the incident electron and the target nucleon are polarized (double-polarization) the scattering cross section depends on two additional functions of Q^2 and ν, g_1 and g_2. In the framework of pQCD these also depend only on x as $Q^2 \rightarrow \infty$. In this limit $g_1(x)$ has a simple interpretation as the sum over the x-dependent polarizations of the various quark flavors. A double-polarization experiment at CERN showed that in the framework of asymptotic QCD only a fraction of the nucleon spin could be attributed to the intrinsic spin of the quarks. These measurements were confirmed by subsequent experiments at CERN, SLAC, and DESY, (see the reviews [2, 3] and references therein). Corrections (higher-twist terms) for finite Q^2 result in excellent fits to the extensive data set for Q^2 down to the order of 2 GeV^2. It is generally accepted that the intrinsic spin of

the quarks accounts for about 25% of the nucleon spin, so that other degrees of freedom, such as gluons and quark orbital angular momentum, must account for the rest.

Until recently, only a few double-polarization experiments were carried out with energies below 25 GeV, an important example being the ground-breaking experiment at SLAC [4] in the late 1970's. More recently, the spin structure function g_1 and its first moment $\Gamma_1(Q^2) = \int g_1(x, Q^2) \, dx$ have become a focus at lower Q^2 and in the resonance region in experiments at SLAC [5], Hermes [6, 7], and JLab [8, 9] to obtain a better understanding of QCD in the confinement regime and to study the phenomenon of duality between the resonance region and the deep inelastic region. The rapidly changing helicity structure of some resonances as a function of Q^2 is expected to have a strong influence on g_1. Double-polarization measurements at lower energies can therefore indicate where pQCD breaks down and determine where multi-parton processes and coherent effects due to nucleon resonance transitions are important.

For inclusive scattering of electrons and protons polarized along the axis of the electron beam, the double-polarization asymmetry is given by:

$$A_{exp} = \frac{\sigma^{\uparrow\downarrow} - \sigma^{\uparrow\uparrow}}{\sigma^{\uparrow\downarrow} + \sigma^{\uparrow\uparrow}} = \sqrt{1 - \epsilon^2} \, \cos\theta_\gamma \left[\frac{A_1 + \eta A_2}{1 + \epsilon R} \right], \quad (1)$$

where $\sigma^{\uparrow\uparrow}$ and $\sigma^{\uparrow\downarrow}$ are the cross sections for the electron and proton spins parallel and anti-parallel, respectively.

The factor $\epsilon = [1 + 2(1 + \nu^2/Q^2)\tan^2(\theta/2)]^{-1}$ is the virtual photon polarization for electron scattering angle θ. The parameter $R = \sigma_L/\sigma_T$ is the ratio of the absorption cross sections for longitudinal and transverse virtual photons. The kinematical factor $\eta = \epsilon\sqrt{Q^2}/(E_0 - \epsilon E')$. The angle between the virtual photon, γ^*, and the beam direction is given by θ_γ.

The photon asymmetries A_1 and A_2 can be written in terms of the virtual photon absorption cross sections as:

$$A_1(x, Q^2) = \frac{\sigma_T^{1/2} - \sigma_T^{3/2}}{2\sigma_T}, \quad A_2(x, Q^2) = \frac{\sigma_{LT}}{\sigma_T}, \quad (2)$$

in which $\sigma_T^{1/2}$ and $\sigma_T^{3/2}$ are transverse cross sections and σ_T is half their sum. The superscripts denote the helicity of the $\gamma^* p$ system. The cross section σ_{LT} arises from longitudinal-transverse interference. In the nucleon resonance region the relative contributions of helicity $1/2$ and $3/2$ vary from one resonance to another and depend strongly on Q^2. The spin structure function g_1 is linearly related to A_1 and A_2 by:

$$g_1(x, Q^2) = \frac{\nu^2}{Q^2 + \nu^2}\left(A_1 + \sqrt{\frac{Q^2}{\nu^2}}A_2\right)F_1(x, Q^2), \quad (3)$$

where F_1 is a structure function appearing in the unpolarized electron scattering cross section.

If the contribution from elastic scattering ($x = 1$) is excluded, Γ_1 vanishes at $Q^2 = 0$, where, in addition, its slope is constrained to be negative by the Gerasimov-Drell-Hearn (GDH) sum rule [10, 11] for absorption of real photons. The validity of the GDH sum rule has been experimentally tested to better than 10% by experiments at Mainz [12] and at ELSA [13]. On the other hand, Γ_1 is known to be positive at high Q^2 [2, 3]. Therefore, the constraints near $Q^2 = 0$ and at high Q^2 imply that Γ_1 must change sign at some low Q^2, where it is expected to be dominated by the nucleon resonances [14, 15].

At low Q^2, meson-baryon dynamics have been treated in chiral perturbation theory by Ji and Osborne [16] and by Bernard, Hemmert, and Meissner [17] to evolve Γ_1 to non-zero values of Q^2. Badelek, Kwieciǹski, and Ziaja [18] have used the generalized vector dominance model and GDH to make predictions for $g_1(x)$ at low Q^2. At high Q^2 the asymptotic value of Γ_1 has been evolved down to $Q^2 = 1~\text{GeV}^2$ by using pQCD and the Operator Product Expansion [19]. Phenomenological approaches, either with explicit inclusion of resonance parameters [20, 21] or with general parametrizations of structure functions [22], have been used to cover the entire Q^2 range.

The present measurements were carried out with 2.6 and 4.3 GeV longitudinally polarized electrons incident on a longitudinally polarized target located at the center of the CLAS detector [23]. A toroidal magnetic field, symmetric about the beam axis, is generated by six super-conducting coils. The coils separate the detector into six independent spectrometers that use wire drift chambers for track reconstruction, scintillation counters for time-of-flight measurements, threshold gas Cerenkov counters, and lead-scintillator electromagnetic calorimeters. Electrons can be detected and identified for momenta down to 0.35 GeV/c and for polar angles from about 8° to 50°. The polarization of the beam, which was measured frequently with a Møller polarimeter, was typically 70%. The beam helicity was flipped at a rate of 1 Hz in a pseudo-random sequence to minimize systematic effects.

A microwave pumped solid nuclear target [24] using the method of Dynamic Nuclear Polarization [25] was built for the CLAS. Its design is similar to those employed in experiments at SLAC [5]. Horizontal cylinders, ~ 1 cm long, were packed with ammonia pellets (either $^{15}\text{NH}_3$ or $^{15}\text{ND}_3$). The cylinders were mounted with their axes along the beam line on a movable ladder, along with an empty cup and a 2.2 mm thick carbon disk. The target cell was immersed in a liquid He bath at T=1.2 K. A pair of super-conducting Helmholtz coils coaxial with the beam generated a uniform 5 T magnetic field in the target volume. A maximum proton polarization of 70% was obtained. During beam irradiation the proton polarization typically dropped gradually to 40%, at which point the target material was removed and replaced in order to restore the original polarization.

Charged particles were identified from the measured momentum and time-of-flight. The Cerenkov counters and calorimeters were used to reduce the π^- contamination in the electron sample to less than 1%. The scattered electrons were binned according to Q^2 and the invariant mass $W = (M^2 + 2M\nu - Q^2)^{1/2}$ of the recoiling hadronic system. For each bin the polarization asymmetry defined in eqn. 1 is:

$$A_{exp} = C_N C_{ps}\frac{1}{P_e P_t}\left(\frac{N^{\downarrow\uparrow} - N^{\uparrow\uparrow}}{N^{\downarrow\uparrow} + N^{\uparrow\uparrow} - N_{bkg}}\right) + A_{RC}, \quad (4)$$

in which P_e and P_t are the averaged polarizations of the electrons and protons, respectively; $N^{\uparrow\uparrow}$ and $N^{\downarrow\uparrow}$ are the number of observed electrons normalized to the total incident beam flux for parallel and anti-parallel beam and target spins; and N_{bkg} is the number of electrons scattered from unpolarized material, which consists of He, ^{15}N, target windows, and foils used to isolate vacuum regions. The factor $C_N = 0.98$ corrects for the contribution of polarized protons in the ^{15}N [5]. The "pair-symmetric" correction C_{ps} and the radiative correction term A_{RC} are discussed below.

The background N_{bkg} accounts for approximately 85% of the detected electrons, and it was determined from an analysis of runs using the carbon target. Comparisons of the carbon and ammonia scattering rates for $W > 1.4$ GeV were used to extract the mass thickness of the

ammonia. The known densities and thicknesses of the materials in the beam-line, along with a parametrization of the ratio of the free proton and neutron cross sections to account for the unpaired proton in ^{15}N, were used to calculate N_{bkg} from the carbon target data.

Eq. 4 does not include corrections for detector acceptance or efficiency since, except for possible changes in the detector between ammonia and carbon runs, these cancel in the ratio. Less than 5% of the data showed short-term localized changes in the detector. The affected regions were removed from the analysis.

The polarization product $P_e P_t$ for each set of runs was extracted directly by comparing the measured asymmetry for elastic scattering to the known elastic ep asymmetry. Two independent procedures were followed. In the first method, the background-subtracted asymmetry was obtained in several Q^2 bins, checked for consistency, and averaged. The second method exploited a limited kinematical range in which both the scattered electron and recoil proton could be detected. The strict correlation in angle and momentum for elastic ep scattering distinguishes it from inelastic ep scattering and from quasi-elastic scattering in nitrogen without subtracting a background spectrum. The two methods were consistent with each other. A typical value was $P_e P_t = (36 \pm 1)\%$.
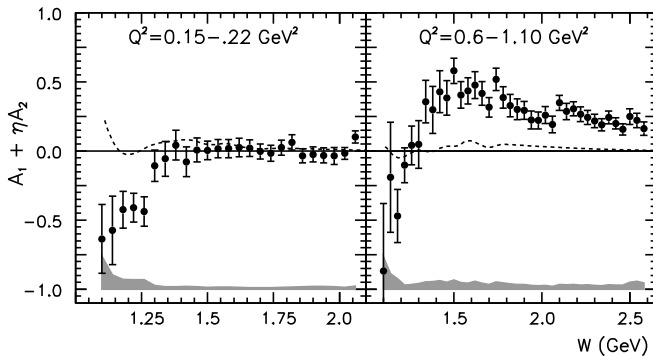

FIG. 1: The photon asymmetry $A_1 + \eta A_2$ vs. the invariant hadronic mass $W(\text{GeV})$ for the proton in two Q^2 bins. The lower Q^2 data were obtained with a beam energy of 2.6 GeV and the higher with 4.3 GeV. The dashed curves show our model estimates of ηA_2. The error bars denote statistical uncertainties and the shaded bands near the bottom of the plot indicate the magnitude of the systematic uncertainties (1σ).

A "pair-symmetric" correction C_{ps} was made for the contribution of $\pi^0 \rightarrow e^+ e^- \gamma$ to the inclusive electron sample. It was determined by measuring the e^+ rate with opposite torus current. Since the correction rises very sharply at high W (low scattered electron energy), we analyzed data only in the kinematic region where the pair-symmetric background was less than 10% of the total electron rate.

Radiative corrections were applied to the experimen-

tal asymmetries using the code RCSLACPOL [5], developed at SLAC and based on the approach of Kuchto and Shumeiko [26] for the internal corrections, and by Tsai [27] for external corrections. We used parametrizations of the world data on unpolarized and polarized structure functions (including our own preliminary asymmetry data) and elastic form factors as input for the radiative correction code. Details of this model will be given in a longer paper.

The model used for radiative corrections was also used to calculate values for A_1, A_2, g_1, g_2, F_1, F_2, and R over the measured region of Q^2 and x. Using the calculated value of R, Eq. 1 was used to obtain $A_1 + \eta A_2$ from the corrected experimental asymmetry defined by Eq. 4. The results for two representative Q^2 bins are shown in Fig. 1. The model values of ηA_2 were generally small, as can be seen from the dashed curves in Fig. 1. These calculated values were used to extract A_1 from the measured A_{exp}. Finally, we used the model for F_1 and A_2, along with Eq. 3, to extract g_1, which is dominated by A_1. The results for g_1 for the proton for five Q^2 bins are shown in Fig. 2. The solid curve shows g_1 calculated from the data parametrization used in RCSLACPOL.
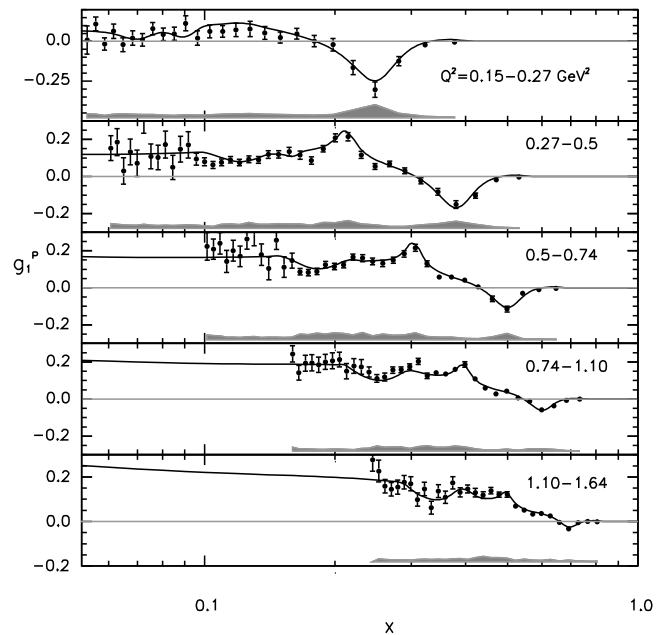

FIG. 2: The polarized structure function $g_1(x)$ vs. x for the proton for five Q^2 bins. The solid lines show the parametrization described in the text. The error bars denote statistical uncertainties and the shaded area at the bottom of each plot indicates the magnitude of the systematic uncertainties (1σ).

We can integrate $g_1(x, Q^2)$ from the lowest measured value of x (with a cut-off ranging from $W=2$ to 2.6 GeV) up to $x = 1$ at each Q^2 to obtain the contribution of our data to the integral Γ_1 (the contribution of elastic scat-

tering is excluded). The results are shown as the closed circles in Fig. 3. The full value of the integral was estimated by using the parametrization for g_1 to estimate the contribution from $x = 10^{-5}$ up to the threshold of our measurements. These extended integrations are shown as open circles. The plot is cut off at $Q^2 = 1.2$ GeV^2 since at higher values more than half the integral is due to the unmeasured region of x. The slope at $Q^2 = 0$
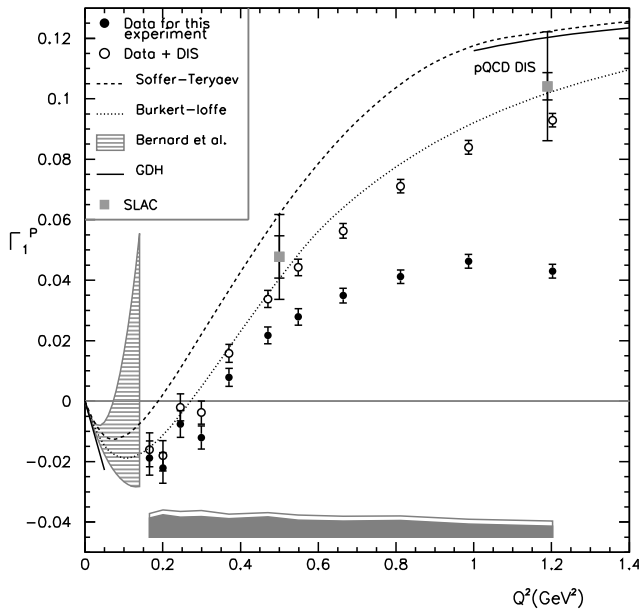

FIG. 3: The first moment Γ_1 vs. Q^2 for the proton. The closed circles are obtained by integrating over our measurements of g_1. The open circles are obtained by using the inclusive scattering model to extend the integral down to $x = 10^{-5}$. The error bars indicate statistical uncertainties. The dark shaded region at the bottom shows the estimated systematic uncertainties (1 σ) for the measured points. The line above the shaded region indicates the systematic uncertainty for the open circles. Measurements from SLAC [5] are shown as shaded squares with the double error bar indicating statistical uncertainty and (statistical + systematic) uncertainties. See the text for an explanation of the curves.

required by the GDH sum rule is indicated by a straight line. Calculations using the light baryon ChPT formulation of Bernard et al. [17] are indicated by a shaded band at $Q^2 < 0.2$ GeV^2 with boundaries that reflect uncertainties in resonance parameters. The pQCD evolution of the deep inelastic scattering measurements to $\mathcal{O}(\alpha_s^3)$ [19] is shown as a line at high Q^2. The calculations of Soffer and Teryaev [22] and Burkert and Ioffe [20] in the intermediate region are also shown. A linear fit to the five points from Q^2=0.20 to 0.47 GeV^2 yields a zero crossing for Γ_1 at $Q^2 = 0.29 \pm 0.03$ GeV^2, where the error includes only the statistical uncertainty and the estimated uncertainty in the DIS contribution added in quadrature. The zero crossing indicates the transition to a distance scale where

non-partonic contributions such as resonance excitations are dominant. Our results for $\Gamma_1(Q^2)$ lie well below the predictions from the pQCD evolution from DIS. They are in better agreement with the model calculations of Ref. [20] that include s-channel baryon resonance excitations explicitly. Thus, we think that it is likely that the lack of explicit inclusion of the resonance contributions in the pQCD evolution gives rise to the discrepancy.

The estimated systematic uncertainties (1 σ) are indicated by the shaded band at the bottom of each plot in the figures. The systematic uncertainty is dominated by the parametrizations of A_2, F_1 and R, which constitute 75% of the total uncertainty at low Q^2 and 50% at high Q^2. The uncertainty is estimated by using alternative parametrizations, as well as by setting R and A_2 to extreme values. The radiative corrections, which also incorporate these models, constitute 20% of the total systematic uncertainty at low Q^2 and 5% at high Q^2. The remaining uncertainty arises largely from livetime calculations and the removal of the nuclear contributions from the ammonia spectra. The systematic uncertainty of the DIS extrapolation for Fig. 3 was estimated by using three different parametrizations for g_1 in the low x region, Simula [21], and the previously mentioned model fitted to world data before 1999 and 2000, respectively.

In summary, our measured asymmetries for inclusive scattering of 2.6 and 4.3 GeV polarized electrons on polarized protons have been used to extract the structure function $g_1(x, Q^2)$ for Q^2 from 0.15 to 1.64 GeV^2. The first moment Γ_1 depends strongly on Q^2, with its sign changing near $Q^2 = 0.3$ GeV^2.

* Deceased
[1] J. Ashman et al., Phys. Lett. B **206**, 364 (1988).
[2] B. Filippone and X. Ji, Adv. in Nucl. Phys. **26**, 1 (2001).
[3] K. Rith, Prog. Part. and Nucl. Phys. **49**, 245 (2002).
[4] G. Baum et al., Phys. Rev. Lett. **45**, 2000 (1980).
[5] K. Abe et al., Phys. Rev. D **58**, 112003 (1998).
[6] A. Airapetian et al., Phys. Lett. B **494**, 1 (2000).
[7] A. Airapetian et al., Phys. Rev. Lett. **90**, 092002 (2003).
[8] M. Amarian et al., Phys. Rev. Lett. **89**, 242301 (2002).

[9] J. Yun et al., Phys. Rev. C **67**, 055204 (2003).

[10] S. Gerasimov, Yad. Fiz. **2**, 598 (1965).

[11] S. Drell and A. Hearn, Phys. Rev. Lett. **16**, 908 (1966).

[12] J. Ahrens et al., Phys. Rev. Lett. **87**, 022003 (2001).

[13] K. Helbing, Nucl. Phys. Proc. Suppl. **105**, 113 (2002).

[14] V. Burkert and Z. Li, Phys. Rev. D **47**, 46 (1993).

[15] D. Drechsel et al., Phys. Rev. **D63**, 114010 (2001).

[16] X. Ji and J. Osborne, J. Phys. G **27**, 127 (2001).

[17] V. Bernard et al., arXiv: hep-ph/0212033.

[18] B. Badelek et al., Eur. Phys. J, C **26**, 45 (2002).

[19] S. Larin and J. Vermaseren, Phys. Lett. B **259**, 345 (1991).

[20] V. Burkert and B. Ioffe, J.E.T.P. **78**, 619 (1994).

[21] S. Simula et al., Phys. Rev. D **65**, 034017 (2002).

[22] J. Soffer and O. V. Teryaev, Phys. Rev. D **51**, 25 (1993).

[23] B. Mecking et al., Nucl. Inst. Meth. **503/3**, 513 (2003).

[24] C. D. Keith et al., Nucl. Instr. Meth. A **501**, 327 (2003).

[25] A. Abragam, *The Principles of Nuclear Magnetization* (Oxford Clarendon Press, 1961).

[26] T. V. Kuchto and N. Shumeiko, Nucl. Phys. **B219**, 412 (1983).

[27] Y. S. Tsai, Rev. Mod. Phys. **46**, 815 (1974).